ORIGINAL ARTICLE

Insight on the structural aspect of ENR-50/TiO$_2$ hybrid in KOH/C$_3$H$_8$O medium revealed by NMR spectroscopy

Omar S. Dahham [a], **Rosniza Hamzah** [a,*], **Mohamad Abu Bakar** [b],
Nik Noriman Zulkepli [a], **Abdulkader M. Alakrach** [a], **Sam Sung Ting** [c],
Mohd Firdaus Omar [d], **Tijjani Adam** [a], **Awad A. Al-rashdi** [e]

[a] Center of Excellence Geopolymer and Green Technology, Faculty of Engineering Technology, Universiti Malaysia Perlis, 02100 Padang Besar, Perlis, Malaysia
[b] Nanoscience Research Laboratory, School of Chemical Sciences, Universiti Sains Malaysia, 11800 Minden, Penang, Malaysia
[c] School of Bioprocess Engineering, Universiti Malaysia Perlis (UniMAP), Kompleks Pengajian Jejawi 3, 02600 Arau, Perlis, Malaysia
[d] School of Materials Engineering, Universiti Malaysia Perlis (UniMAP), Kompleks Pengajian Jejawi 2, 02600 Arau, Perlis, Malaysia
[e] Chemistry Department, Umm Al-Qura University, Al-qunfudah University College, Al-qunfudah Center for Scientific Research (QCSR), Saudi Arabia

Abstract The ring-opening reactions (ROR) of epoxide groups in epoxidized natural rubber/titania (ENR-50/TiO$_2$) hybrid in potassium hydroxide/isopropanol medium were examined using NMR spectroscopy and supported by the FTIR technique. The thermal behaviour of the hybrid was also studied using TG/DTG and DSC analyses. The ^{1}H NMR results suggested that 16.82% of ROR occurred in the hybrid, while the ^{13}C NMR results exhibited five new peaks at δ 19.5, 71.0, 73.7, 91.7 and 94.4 ppm in the hybrid. 2D NMR, such as HMQC, HMBC and COSY techniques, further scrutinized these assignments. The FTIR spectrum exhibited Ti-O-C characteristics via the peak at 1028 cm^{-1}. The TG/DTG results showed four steps of thermal degradation at 44–148, 219–309, 331–489 and 629–810 °C due to the existence of Ti moieties along with a polymer

* Corresponding author.
  E-mail address: rosnizahamzah@unimap.edu.my (R. Hamzah).
Peer review under responsibility of King Saud University.

Production and hosting by Elsevier

chain mixture (intact and ring-opened epoxide groups) of ENR-50, which in turn led to an increase in the T$_g$ value of the hybrid to 27 °C compared to that of purified ENR-50 at −17.72 °C.

1. Introduction

The idea of producing a unique material by combining the properties of organic and inorganic materials has emerged in the last few decades. The first application of organic/inorganic hybrids was in the paints industry, where metal oxides, such as titanium dioxide (TiO$_2$), were added into organic mixtures, such as surfactants or solvents (Judeinstein and Sanchez, 1996). However, the name hybrid was not common at that time. The development of the structure of organic/inorganic hybrids has continued in conjugation with the development of the polymer industry. Inorganic materials, such as talcs, metal oxides, clays, and minerals, are usually added into polymers in order to enhance the properties of the composites (Judeinstein and Sanchez, 1996; Kango et al., 2013).

The term organic/inorganic hybrid has emerged only recently, when studies have focused more on advanced materials (Judeinstein and Sanchez, 1996; Sanchez et al., 2011). Currently, studies on the networks of organic/inorganic hybrids, particularly nano-scale hybrids, have become a growing field of study (Sanchez et al., 2011). This type of material is considered unconventional and advanced, which could be used in a wide range of applications in various fields such as electronics, optics, mechanics, ionics, and biology (Sanchez et al., 2005). At first sight, organic/inorganic hybrids are considered as biphasic materials, where the different phases are mixed at the nanometre scale. However, it is clear that the characteristics of these hybrids are not just the sum of the individual contributions from both phases; the role of inner interfaces is predominant (Judeinstein and Sanchez, 1996).

The sol-gel technique is a process of chemical synthesis, which is widely used for inorganic material preparation such as ceramics and glasses. The distinctive characteristics of this technique, such as low temperature processing, provides good opportunity to produce controlled and pure structure of organic/inorganic hybrids through incorporation between the low molecular weight organic molecules and the inorganic moieties (Sanchez et al., 2005; Wen and Wilkes, 1996; Pandey and Mishra, 2011). In the last few decades, organic/inorganic hybrids prepared by the sol-gel technique have received much attention in many fields, such as polymer chemistry, physics, ceramics, and organic/inorganic chemistry. The preparation, characterization, and applications of organic/inorganic hybrids have become a fast-growing research area in materials science. The key driving force behind the intensive studies in this area is the unique properties of these hybrids, which the conventional composites do not have (Judeinstein and Sanchez, 1996). For instance, unlike the conventional macroscale composites that have millimetre or micrometre scale domain size, the majority of the organic/inorganic hybrids are nanoscopic, with the physical constraint of different nanometres, and usually, the minimum size of the phases or components starts from 1 to 100 nm. Consequently, these materials are often still optically transparent despite the exis-

tence of a microphase interface. Through the combinations between organic and inorganic components concurrently with suitable processing methods, many kinds of primary and/or secondary bonding may occur, producing materials with good structural, optical and even electrical properties.

In the last few years, metal oxides, such as titanium dioxide (TiO$_2$), have received much attention due to the numerous real and potential applications (Macwan et al., 2011). TiO$_2$ has a high refractive index (RI), which is used widely in optical designs such as optoelectronic fabrication, ophthalmic lenses, optical adhesives, light-emitting-diodes encapsulation, and high reflective and antireflection coatings (Lü and Yang, 2009; Ochi et al., 2010; Tao et al., 2011). TiO$_2$ can also be used to produce thin dielectric materials, which are used in storage capacitors and dynamic random access memory. In addition, TiO$_2$ is considered a good source for photocatalytic detoxification of organic pollutants in water and wastewater treatments (da Silva et al., 2006; Nawi et al., 2003). However, TiO$_2$ has some disadvantages, such as high density and low flexibility, which may restrict its uses in many applications. TiO$_2$ can successfully be used to produce polymer/TiO$_2$ composites or hybrids with good dielectric properties, high thermal stability, and excellent mechanical and optical properties (Lü and Yang, 2009). Several studies found in the literature studied the effect of TiO$_2$ addition into many different polymers, such as fluoropolymer (He et al., 2010), acrylic resin (Xiong et al., 2004), polyimide (Chiang et al., 2004), poly(9-vinylcarbazole) (Barlier et al., 2007), poly(acrylic acid) (Chen et al., 2007), poly (methyl methacrylate) (Cao et al., 2013), cellophane membrane (Wetchakun and Phanichphant, 2008) and others (Lou et al., 2010; Buzarovska and Grozdanov, 2012; Charpentier et al., 2012; Ouyang et al., 2012; Babazadeh et al., 2012).

On the other hand, the increasing interest in the science and technology of epoxidized natural rubber (ENR) in various fields such as polymer blends (Mohamad et al., 2006), polymer modifications (Noriman et al., 2010), polymer composites (Bakar et al., 2008) and advanced green materials (Han et al., 2004; Lee et al., 2005; Mishra et al., 2007) make it inevitable to understand the detailed structure of ENR. Thus, the combination of ENR and TiO$_2$ will open up new propositions in the rubber industry. There are limited studies on ENR-50/TiO$_2$ nanocomposites found in the literature, and most of those studies focused on the thermal and mechanical properties only.

Our current work focused on the characterization of the chemical structure of ENR-50/TiO$_2$ hybrid in a potassium hydroxide/isopropanol solution to prove the formation of new covalent bonds between TiO$_2$ and ENR-50 using 1D/2D NMR spectroscopy and supported with the FTIR technique. There is a dearth of studies using NMR spectroscopy to demonstrate the hybrid formation *via* the analysis of covalent bonds. Therefore, it is important to extend the scope of the characterization techniques to remove doubts in the results and investigate the chemical structure of the newly formed hybrid.

2. Experimental

2.1. Materials

Epoxidized natural rubber (ENR-50) was provided from the Rubber Research Institute (RRI), Malaysia. Titania precursors (Titanium-IV isopropoxide 98%) were purchased from Merck, Germany. *n*-Hexane, toluene, 2-propanol, and chloroform were purchased from Systerm, Malaysia. Deuterated chloroform (CDCl3) and Tetrahydrofuran (THF) were purchased from Fluka Chemicals, Switzerland. All the materials were used in this work without any further purification unless otherwise stated.

2.2. Preparative procedure

All experiments in this work were carried out at atmospheric pressure unless otherwise stated. These experiments involved three main stages to synthesize the ENR-50/TiO$_2$ hybrid.

2.2.1. ENR-50 purification
The first step of purification was the swelling of 20 g of ENR-50 in 400 mL of chloroform and then stirring it for 24 h at 25 °C. After that, a cotton gauze pack was used to filtrate the solution by separating the high from the low molecular weight ENR-50. The latter was precipitated in *n*-hexane and then stirred using a glass rod. The precipitate stuck on the glass rod was moved to a Teflon petri dish and then dried using a vacuum oven at 50 °C for 48 h. The samples after drying represented the purified ENR-50 (Hamzah et al., 2016).

2.2.2. ENR-50 base treatment
In a typical preparation, 0.21 M (14.09 mg mL^{-1}) of potassium hydroxide/isopropanol (KOH/IPA) solution was prepared by dissolving 1.41 g (21.35 × 10^{-3} mol) of KOH pellets in 100 mL of IPA. After that, 200 mg (1.32 × 10^{-3} mol) of purified ENR-50 obtained from stage 1 (Section 2.2.1) was dissolved and stirred in 40 mL of toluene. Approximately 10 mL of KOH stock solution was added to the mixture in order to adjust the pH of the solution to 12. The mixture was refluxed at 85 °C for 3 h and then left to cool to 60 °C (Dahham et al., 2017).

2.2.3. ENR-50/TiO$_2$ hybrid synthesis
A 1.32 × 10^{-3} M (3.82 × 10^{-3} mg mL^{-1}) Ti(OCH$_2$CH$_2$CH$_3$)$_4$ solution was prepared by adding 38.18 mg (1.32 × 10^{-4} mol) of Ti(OCH$_2$CH$_2$CH$_3$)$_4$ precursor in 10 mL of IPA. After that, approximately 10 mL of the Ti(OCH$_2$CH$_2$CH$_3$)$_4$ solution was slowly added dropwise to 44 mL of the base treated ENR-50 prepared in stage 2 (Section 2.2.2) at 60 °C. Upon completion, the mixture was kept at 60 °C for 24 h. The reaction mixture was washed with 150 mL of water until the washing attained a neutral pH. The resultant reaction mixture was cast onto a Teflon dish and kept in a fume cupboard for 48 h for drying. A vacuum oven was then used for further drying at 50 °C for 24 h. The sample was characterized using 1D/2D NMR and FTIR spectroscopy techniques. The thermal characteristics of the sample were characterized using TG/DTG and DSC analyses.

2.3. Measurements and characterization techniques

Nuclear magnetic resonance (NMR) spectroscopy (Bruker Avance model, 500-MHz) was used to analyse the specimen in CDCl$_3$ solvent at 25 °C. Before conducting the analysis, the specimen was swelled for 4 days in the NMR tube. After that, 10.00 mg of the prepared specimen was used for proton (^{1}H-) NMR analysis, and 50.00 mg of the prepared specimen was used for carbon (^{13}C-) NMR analysis and 2D NMR analysis including heteronuclear multiple quantum coherence (HMQC), heteronuclear multiple bond coherence (HMBC), and correlation spectroscopy (COSY) analyses. The spectra range and scan number of ^{1}H- and ^{13}C NMR analyses were 15–0 ppm with 16 scans and 200–0 ppm with 15,000 scans respectively.

The Fourier transform infrared (FTIR) spectroscopy model, *Perkin-Elmer 2000-FTIR,* was used in this work. The specimen was prepared by drop casting the redispersed residue as a film onto a zinc selenide (ZnSe) window. The spectra were recorded at the 4000–600 cm^{-1} wavenumber range.

The thermogravimetric analyser model Perkin Elmer TGA-7 was used to investigate the thermal stability of the specimen. The test was conducted by heating 10.00 mg of the specimen from room temperature up to 900 °C with a 20 °C/min heating rate under a nitrogen atmosphere.

Moreover, a Perkin Elmer Pyris-6 (Shelton CT) differential scanning calorimeter was used for further thermal characterization of the specimen. Approximately 10.00 mg of specimen was placed in the aluminium pan of the DSC instrument. The test was conducted under a nitrogen atmosphere at the temperature range of −50 to 140 °C with a 20 °C/min heating rate. In the test, the specimen was heated from −50 to 140 °C and held at 140 °C for 1 min and then cooled to −50 °C and held for 5 min. After 5 min, the specimen was reheated to 140 °C again.

2.4. Theoretical treatments

The epoxide amount and the ring opening reaction percentage of a specimen were determined based on ^{1}H NMR analysis using Eqs. (1) and (2), respectively (Ochi et al., 2010; Mas Haris and Raju, 2014; Caldeira et al., 2012; Li et al., 1998), where I$_{5.2}$ and I$_{2.7}$ are the methine proton integrated areas of isoprene and epoxidized isoprene, respectively. I$_{2.7}$ is selected because it is the initial reactive site for the reaction and for purified ENR-50, and the integrated area of this peak is one proton (Eq. (1)). The integrated area at I$_{2.7}$ after reaction is generally less than I$_{2.7}$ before reaction, whereas I$_{5.2}$ remains similar before and after the reaction. This is because the methine proton of isoprene is not involved in this reaction. In Eq. (2), the ring opening percentage in the specimen is a deduction of the epoxide percentage left in the ring opened specimen after reaction from the epoxide percentage in purified ENR-50.

$$\% \text{ Epoxide in sample} = I_{2.7} * 100\% / I_{2.7} * I_{5.2} \qquad (1)$$
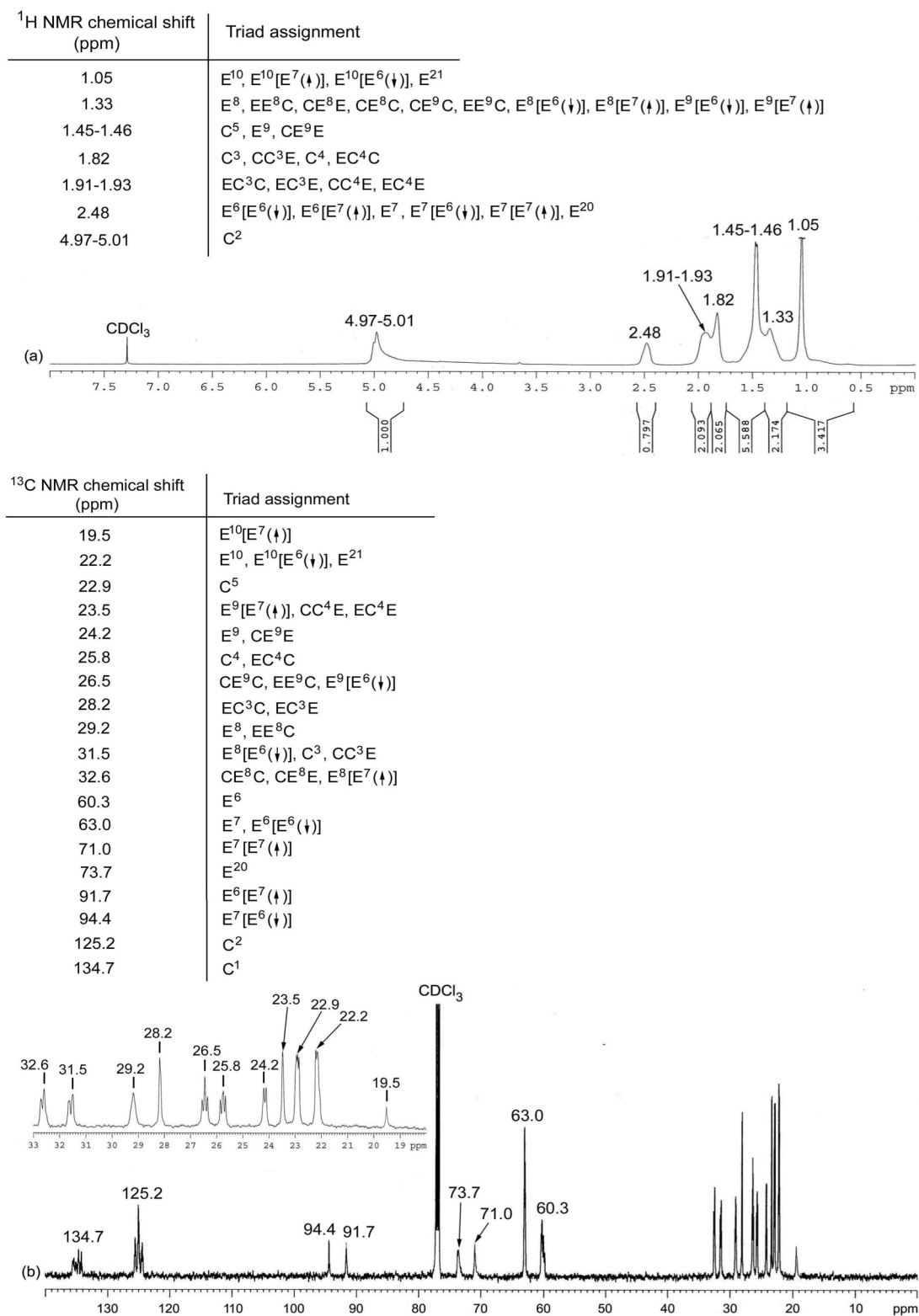
^{1}H NMR chemical shift (ppm)	Triad assignment
1.05	E^{10}, E^{10}[E^7(↓)], E^{10}[E^6(↓)], E^{21}
1.33	E^8, EE^{8}C, CE^{8}E, CE^{8}C, CE^{9}C, EE^{9}C, E^8[E^6(↓)], E^8[E^7(↓)], E^9[E^6(↓)], E^9[E^7(↓)]
1.45–1.46	C^5, E^9, CE^{9}E
1.82	C^3, CC^{3}E, C^4, EC^{4}C
1.91–1.93	EC^{3}C, EC^{3}E, CC^{4}E, EC^{4}E
2.48	E^6[E^6(↓)], E^6[E^7(↓)], E^7, E^7[E^6(↓)], E^7[E^7(↓)], E^{20}
4.97–5.01	C^2

^{13}C NMR chemical shift (ppm)	Triad assignment
19.5	E^{10}[E^7(↓)]
22.2	E^{10}, E^{10}[E^6(↓)], E^{21}
22.9	C^5
23.5	E^9[E^7(↓)], CC^{4}E, EC^{4}E
24.2	E^9, CE^{9}E
25.8	C^4, EC^{4}C
26.5	CE^{9}C, EE^{9}C, E^9[E^6(↓)]
28.2	EC^{3}C, EC^{3}E
29.2	E^8, EE^{8}C
31.5	E^8[E^6(↓)], C^3, CC^{3}E
32.6	CE^{8}C, CE^{8}E, E^8[E^7(↓)]
60.3	E^6
63.0	E^7, E^6[E^6(↓)]
71.0	E^7[E^7(↓)]
73.7	E^{20}
91.7	E^6[E^7(↓)]
94.4	E^7[E^6(↓)]
125.2	C^2
134.7	C^1

Fig. 1 (a) ^{1}H- and (b) ^{13}C NMR spectra of ENR/TiO$_2$ hybrid (in CDCl$_3$).

Table 1 ^{1}H-, ^{13}C NMR chemical shifts and HMQC, HMBC and COSY spin coupling correlations of ENR/TiO$_2$ hybrid.

^{1}H Chemical shift, δ (ppm)		^{13}C Chemical shift, δ (ppm)		HMQC triad assignment	Coupling correlation of the middle unit, δ (ppm)	
Base treated ENR-50	ENR/TiO$_2$ hybrid (base condition)	Base treated ENR-50	ENR/TiO$_2$ hybrid (base condition)		HMBC	COSY
-	1.05	-	19.5	E^{10} [E^7(↑)]	None	None
1.30	1.05	22.2	22.2	E^{10}	None	None
1.30	1.05	22.2	22.2	E^{21}	73.7 (E^{20})	2.48 (E^{20})
-	1.05	-	22.2	E^{10} [E^6(↓)]	None	None
1.57	1.33	27.0	26.5	CE^{9}C, EE^{9}C	60.3 (E^6), 63.0 (E^7)	2.48 (E^7)
1.57	1.33	29.7	29.2	EE^{8}C, E^8	22.2 (E^{10}), 60.3 (E^6), 63.0 (E^7)	None
1.57	1.33	33.1	32.6	CE^{8}C, CE^{8}E	22.2 (E^{10}), 60.3 (E^6), 63.0 (E^7)	None
-	1.33	-	32.6	E^8 [E^7(↑)]	19.5 (E^{10}), 32.6 (E^6), 71.0 (E^7)	None
-	1.33	-	26.5	E^9 [E^6(↓)]	63.0 (E^6), 94.4 (E^7)	2.48 (E^7)
-	1.33	-	31.5	E^8 [E^6(↓)]	22.2 (E^{10}), 63.0 (E^6), 94.4 (E^7)	None
-	1.33	-	23.5	E^9 [E^7(↑)]	91.7 (E^6), 71.0 (E^7)	2.48 (E^7)
1.69	1.45-1.46	23.3	22.9	C^5	31.5 (C^3), 125.2 (C^2), 134.7 (C^1)	None
1.69	1.45-1.46	24.6	24.2	CE^{9}E, E^9	60.3 (E^6), 63.0 (E^7)	2.48 (E^7)
2.06	1.82	26.2	25.8	C^4, EC^{4}C	125.2 (C^2), 134.7 (C^1)	4.97-5.01 (C^2)
2.06	1.82	26.2	31.5	C^3, CC^{3}E	22.9 (C^5), 125.2 (C^2), 134.7 (C^1)	None
2.18	1.91-1.93	23.9	23.5	CC^{4}E, EC^{4}E	125.2 (C^2), 134.7 (C^1)	4.97-5.01 (C^2)
2.18	1.91-1.93	28.7	28.2	EC^{3}C, EC^{3}E	22.9 (C^5), 125.2 (C^2), 134.7 (C^1)	None
-	-	60.8	60.3	E^6	-	-
2.73	2.48	64.5	63.0	E^7	22.2 (E^{10}), 29.2 (E^8)	1.45-1.46 (E^9)
2.73	2.48	73.7	73.7	E^{20}	22.2 (E^{21})	1.05 (E^{21})
-	-	-	63.0	E^6 [E^6(↓)]	-	-
-	2.48	-	71.0	E^7 [E^7(↑)]	23.5 (E^9)	1.45-1.46 (E^9)
-	-	-	91.7	E^6 [E^7(↑)]	-	-
-	2.48	-	94.4	E^7 [E^6(↓)]	23.5 (E^9)	1.45-1.46 (E^9)
5.13-5.17	4.97-5.01	125.1	125.2	C^2	22.9 (C^5) 25.8 (C^4) 31.5 (C^3)	1.82 (C^4)
-	-	134.7	134.7	C^1	-	-

Note: New peaks of ENR/TiO$_2$ hybrid are highlighted in green for Ti attached to E^7(↑) and in yellow for Ti attached to E^6(↓).
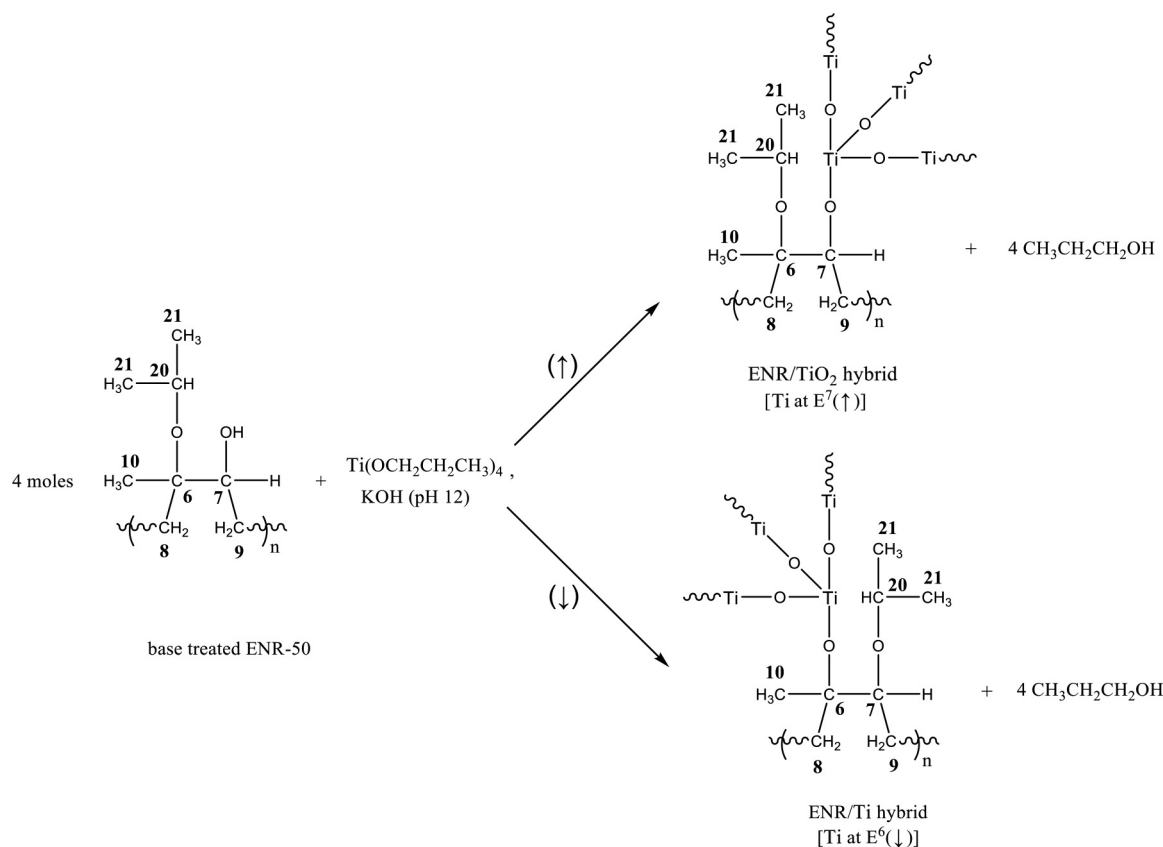
Fig. 2 Proposed formations of ENR/TiO$_2$ hybrids from base treated ENR-50 and its carbon numbering.

$$\% \text{ Ring opening in sample} = (\% \text{ epoxide in purified ENR-}50$$
$$- \% \text{ epoxide in sample})$$
$$* 100\%/\% \text{ epoxide in purified ENR-}50$$
$$(2)$$

3. Results and discussion

3.1. NMR

3.1.1. ^1H- and ^{13}C NMR

The ^{1}H- and ^{13}C NMR spectra of the ENR/TiO$_2$ hybrid are shown in Fig. 1, and the respective chemical shifts are tabulated in columns 2 and 4 of Table 1. From Fig. 1(a), the chemical shifts of the ENR/TiO$_2$ hybrid are shifted to the upfield region compared to base treated ENR-50 (Dahham et al., 2017) due to the presence of Ti moieties in the hybrid. Thus, the chemical shifts of C^2 and E^7 appear slightly upfield at δ 4.97–5.01 and 2.48 ppm, respectively. Based on the proton integrals of C^2 and E^7, Eqs. (1) and (2) were used to measure the extent of the ring opening reaction in this hybrid. It shows that the level of the ring opening reaction remained at 16.82% and is similar to base treated ENR-50 (Dahham et al., 2017). This indicates that the presence of Ti moieties does not affect (increase/decrease) the level of epoxide ring opening reaction of ENR-50 in the base treated ENR-50.

In the ENR/TiO$_2$ hybrid, two regions of hydroxyl/methine proton as seen in the previous base treated ENR-50 (Dahham et al., 2017) have now disappeared. The absence of this hydroxyl/methine proton indicates that the hydroxyl group is reactive towards the Ti precursor. The hydroxyl group of ring opened epoxide is involved in the reaction with the Ti precursor as given in Fig. 2. Furthermore, it implies the equal preference of Ti moieties to attach at E^6(↓) and E^7(↑) of the ring opened epoxide of ENR. Thus, in the formation of ENR/TiO$_2$, the Ti precursor attack is not specific as long as it is reacted to the reactive hydroxyl groups.

The methyl protons of E^{10} of the hybrid and ENR and the methyls of isopropyl (IP) E^{21} are simultaneously located at δ 1.05 ppm. The shape of the peak is almost similar to the base treated ENR-50 (Dahham et al., 2017), except it is less intense. The peak at δ 1.33 ppm corresponds to the methylene protons of E^8 and part of E^9 of ENR as well as E^8 and E^9 of the ENR/TiO$_2$ hybrid. The remaining part of E^9 of the non-hybrid is shown at δ 1.45–1.46 ppm, together with the methyl protons of C^5. The rest of the methylene protons of C^3 and C^4 are at δ 1.82 and 1.91–1.93 ppm. The peak at δ 2.48 ppm belongs to the methine proton of E^7 of the hybrid and ENR as well as the methine proton E^{20} of IP. The methine proton of C^2 remains at δ 4.97–5.01 ppm.

The ^{13}C NMR spectra of ENR/TiO$_2$ are shown in Fig. 1(b) and their chemical shifts are tabulated in column 4 of Table 1. There are two types of ENR/TiO$_2$ hybrids from the formation of C—O—Ti bond: either the Ti atom is attached at E^6(↓) or E^7(↑) carbons. For simplification purposes, in order to denote the respective carbon such as the methyl carbon of E^{10} for Ti attached to E^7, it is abbreviated as E^{10} [E^7(↑)]. This also applies
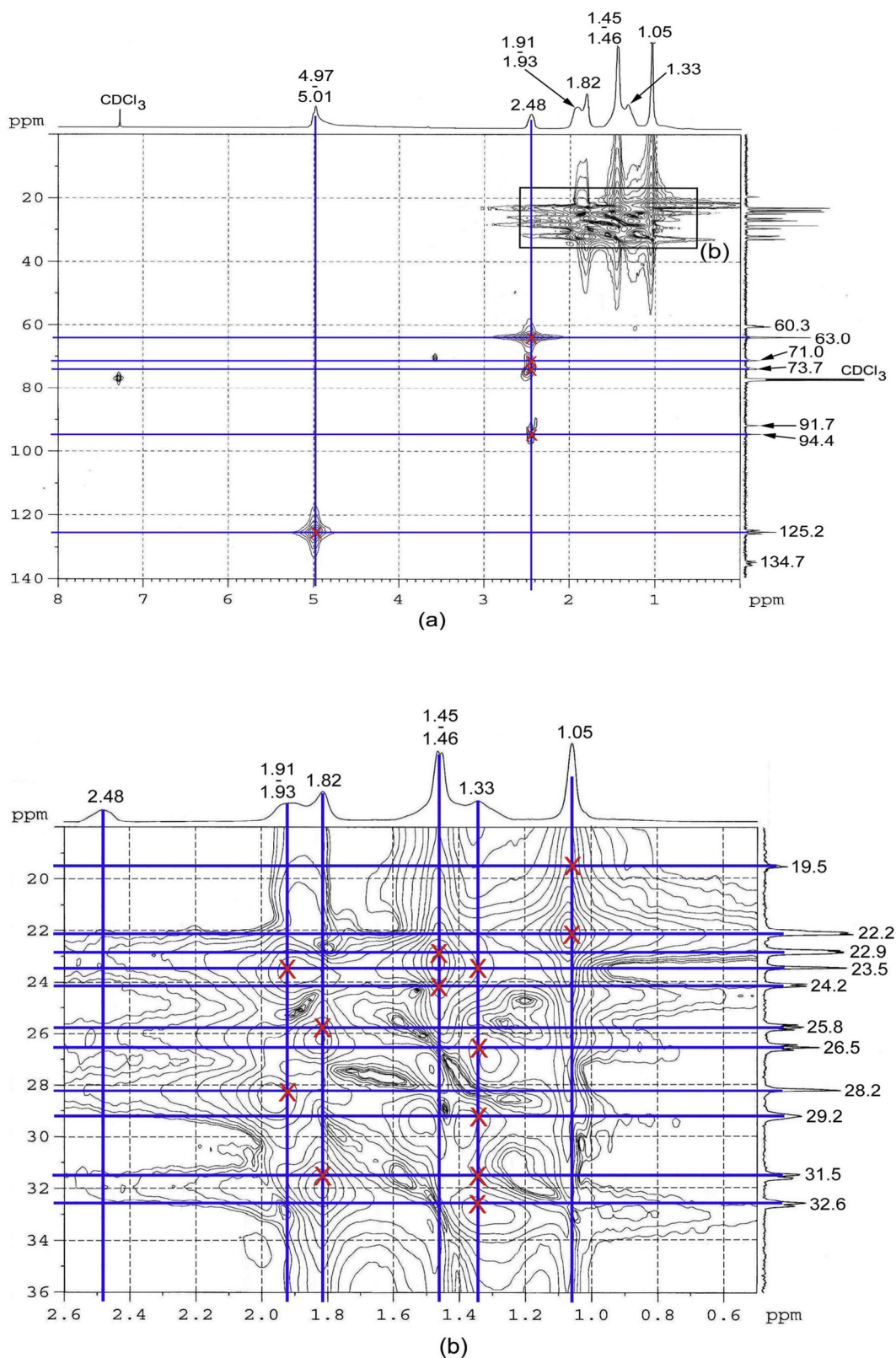
Fig. 3 HMQC spectra of (a) ENR/TiO2 hybrid and (b) enlargement of the boxed region in (a).

to the other protons of carbon in the ENR/TiO$_2$ hybrid. The new peaks due to the attachment of Ti at E^6 or Ti at E^7 are highlighted Table 1in yellow and green, respectively.

Generally, the ENR/TiO$_2$ hybrids exhibit 5 new peaks at δ 19.5, 71.0, 73.7, 91.7 and 94.4 ppm compared to purified ENR-50. The peak at δ 19.5 ppm corresponds to E^{10} [E^7(↑)]. It
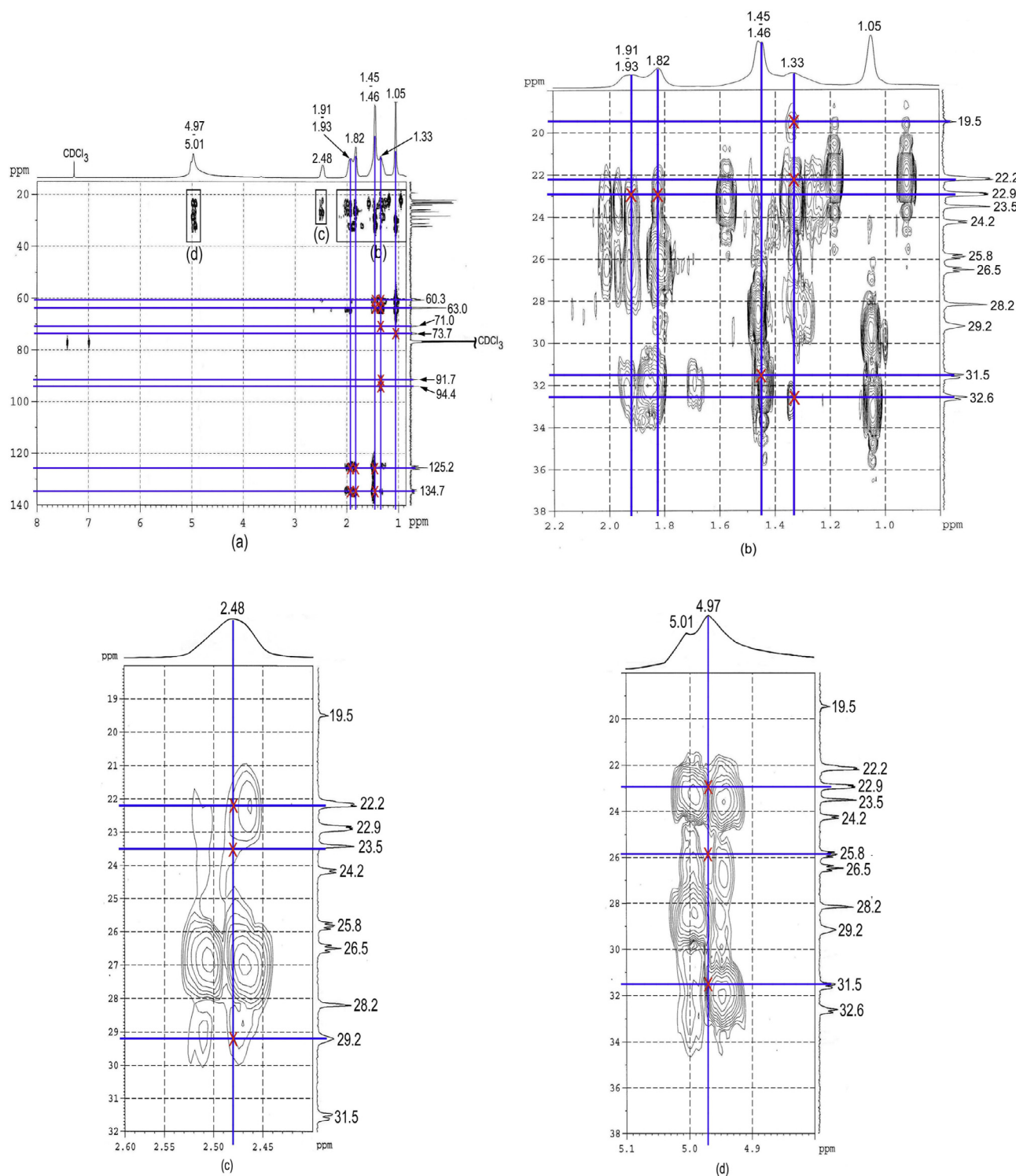
Fig. 4 HMBC spectra of (a) ENR/TiO₂ hybrid and (b, c, d) enlargement of the boxed region in (a).

appears at the most upfield region compared to E^{10} [$E^6(\downarrow)$], which is shown together with E^{10} of the non-hybrid and E^{21} at δ 22.2 ppm. The E^{10} carbon is influence by vicinal E^6 carbon regardless of whether it is the hybrid or non-hybrid. Thus, E^{10} [$E^7(\uparrow)$] is more upfield than E^{10} [$E^6(\downarrow)$].

The peak at δ 71.0 ppm belongs to E^7 [$E^7(\uparrow)$], which is located upfield compared to E^7 [$E^6(\downarrow)$] and appears at δ 94.4

ppm. This is because the carbon of E^7 [$E^7(\uparrow)$] is directly bonded to Ti via C—O—Ti. It is similarly argued for E^{10} carbon. The peak at δ 91.7 ppm belongs to E^6 [$E^7(\uparrow)$]. It appears downfield compared to E^6 [$E^6(\downarrow)$], which is shown simultaneously with E^7 of purified ENR-50 at δ 63.0 ppm. The methine carbon of E^{20} is shown at δ 73.7 ppm, which is similar to base-treated ENR-50 (Dahham et al., 2017). The chemical shifts for the
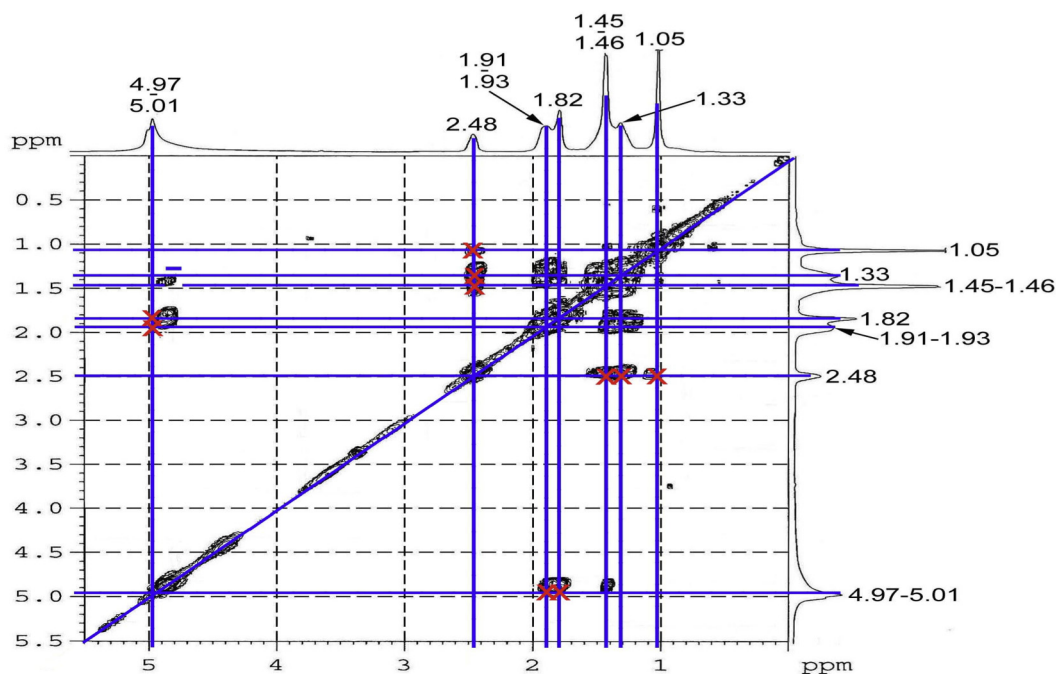
Fig. 5   COSY spectra of ENR/TiO$_2$ hybrid.

methylene carbon of E^8 [E^6(↓)] and E^8 [E^7(↑)] appear at δ 31.5 and 32.6 ppm, respectively, while the chemical shifts for the methylene carbon of E^9 [E^7(↑)] and E^9 [E^6(↓)] are at δ 23.5 and 26.5 ppm, respectively.

3.1.2. HMQC

Fig. 3 shows the HMQC spectra of the ENR/TiO$_2$ hybrid, and the triad assignments are tabulated in column 5 of Table 1. The HMQC analysis is mainly conducted to identify the correlation of E^{10}, E^7, E^8 and E^9 of the ENR/TiO$_2$ hybrid arising from both [E^6(↓)] and [E^7(↑)]. Similar to the Ti in acid-treated ENR/TiO$_2$ (Dahham et al., 2018), Ti here is an electropositive atom that shields the electron density of the nearby group. Thus, the formation of the ENR/TiO$_2$ hybrid via C—O—Ti bond will influence the correlation contour of the obtained hybrid compared to purified ENR-50 and base-treated ENR-50. In general, the correlation contour of the hybrid [E^6(↓)] appears downfield compared to [E^7(↑)]. This is due to the direct attachment of Ti to E^6 via C—O—Ti bond and applies to E^{10}, E^7 and E^9. However, the correlation contour of E^8 is different, where [E^6(↓)] is upfield compared to [E^7(↑)], which is downfield. This is due to the E^8 being vicinal to E^6. The E^6 is at upfield for [E^6(↓)] and for [E^7(↑)]. The vicinal bond between E^8 and E^6 influences the correlation contour of E^8.

3.1.3. HMBC

The HMBC correlation spectra of the ENR/TiO$_2$ hybrid are shown in Fig. 4, and the relevant data are tabulated in column 6 of Table 1. The proton signals at δ 1.33 and 2.48 ppm are individually assigned to scrutinize the coupling correlations of E^8, E^9, and E^7 of the formed hybrid. Similar to the HMBC spectra of acid-treated ENR/TiO$_2$ hybrid (Dahham et al., 2018), the coupling correlation obtained is of the middle unit

of the triad sequence only. The ^{1}H signal at δ 1.33 ppm correlates with ^{13}C signals at δ 19.5, 32.6 and 71.0 ppm for E^8 [E^7(↑)], while E^8 [E^6(↓)] correlates with the ^{13}C signals at δ 22.2, 63.04 and 94.4 ppm. The correlation of E^9 [E^6(↓)] is obtained via the correlation of ^{1}H signal at δ 1.33 ppm to the ^{13}C signals at δ 63.0 and 94.4 ppm. However, for E^9 [E^7(↑)], the correlation is within the ^{13}C signals at δ 71.0 and 91.7 ppm. The coupling correlation of E^7 [E^7(↑)] is at the upfield region compared to E^7 [E^6(↓)]. Thus, the spectra affirmatively assigned the coupling correlation of the ENR/TiO$_2$ hybrid.

3.1.4. COSY

The COSY of the ENR/TiO$_2$ hybrid is shown in Fig. 5 and was conducted to evaluate the representation of the ^{1}H NMR signals at δ 1.05, 1.33, 1.45–1.46, 1.82, 1.91–1.93 and 2.48 ppm. The assigned correlation is to the middle unit of the triad sequence and tabulated in column 7 in Table 1.

The signal at δ 1.05 ppm correlates with the signal at δ 2.48 ppm to the methine proton of IP E^{20}. The signals of methylene protons of E^9 at δ 1.33 and 1.45–1.46 ppm correlate to the methine proton of E^7 [E^6(↓)] or [E^7(↑)] as well as E^9 of the purified ENR-50 at δ 2.48 ppm. Similar to the purified ENR-50, the methylene protons of C^4 at δ 1.82 and 1.91–1.93 ppm correlate to the methine proton of C^2 at δ 4.97–5.01 ppm. The signal at δ 2.48 ppm correlates with the signals at δ 1.05 and 1.45–1.46 ppm, and the signal at δ 4.97–5.01 ppm correlates to the signal at δ 1.82 ppm.

Based on the COSY spectra of the ENR/TiO$_2$ hybrid, the new signals at δ 1.33 and 2.48 ppm belong to the formed hybrid. The signal at δ 1.33 is for the methylene protons of E^9 [E^6(↓)] or E^9 [E^7(↑)], and the signal at δ 2.48 ppm is for the methine proton of E^7 [E^7(↑)]. These findings further confirmed the HMQC results above.
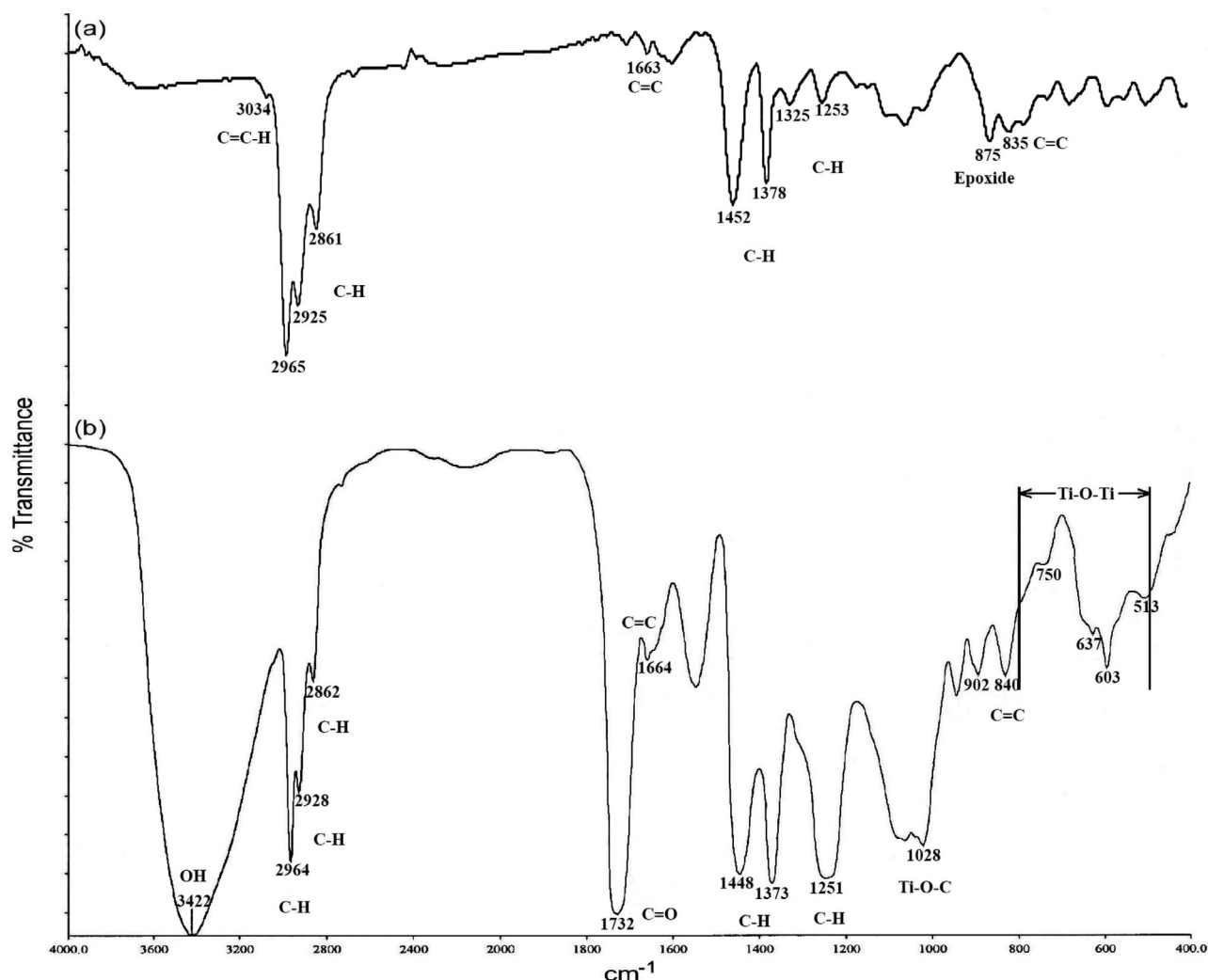
Fig. 6 FTIR spectra of (a) Purified ENR and (b) ENR/TiO$_2$ hybrid.

3.2. FTIR spectroscopy

The FTIR spectra of purified ENR-50 and the ENR/TiO$_2$ hybrid are shown in Fig. 6a and b respectively. It can be observed that the presence of Titania in the hybrid has significantly increased the intensity of broad —OH group peak at 3420–3425 cm^{-1} forming Ti-OH bond, a similar characteristic of —OH peaks in the acid-treated ENR/TiO$_2$ hybrid was observed (Dahham et al., 2018). However, the —OH peak overlapped with the intermolecular hydrogen bond peak in ENR-50 in the range of 3400–3200 cm^{-1} (Conley, 1972). The peak at 1028 cm^{-1} corresponds to the formation of the Ti—O—C bond of the hybrid, and the Ti—O—Ti peak is observed at 800–500 cm^{-1} (Ochi et al., 2010). Similar to acid-treated ENR/TiO$_2$ hybrid (Dahham et al., 2018), the characteristic of ENR in the ENR/TiO$_2$ hybrid is demonstrated by peaks at 2964, 2928, 2862, 1448, and 1373 cm^{-1} for C—H and 1664 and 840 cm^{-1} for C=C. The epoxide group of the ENR-50 peak typically at 870–880 cm^{-1} is not observed in the hybrid due to overlapping with the peak of C=C at 840 cm^{-1}.

3.3. TG/DTG analyses

The thermogravimetric (TGA) and derivative thermogravimetric (DTG) thermograms of purified ENR-50 and the ENR/TiO$_2$ hybrid are depicted in Fig. 7(a) and (b), respectively. In general, the purified ENR-50 shows a single step of thermal degradation between 342 and 481 °C with approximately 38% rapid weight loss at 402 °C. The total weight loss of the rubber sample is approximately 99% due to the pyrolysis process of the rubber matrix, which caused hydrocarbon decomposition in a nitrogen atmosphere (Mas Haris and Raju, 2014). The amount of carbon residue of the rubber sample beyond 490 °C is approximately 1%. The ENR/TiO$_2$ hybrid shows 4 steps of thermal degradation over the temperature range studied at 44–148, 219–309, 331–489 and 629–810 °C.

The first degradation is due to the residue removal of moisture and trapped organic from the gel network of the hybrid (Caldeira et al., 2012). The second degradation is due to the hydroxyl groups removal from the hybrid structure (Caldeira et al., 2012). The third degradation represents the ENR-50 degradation and the acetate group residual. During pyrolysis,
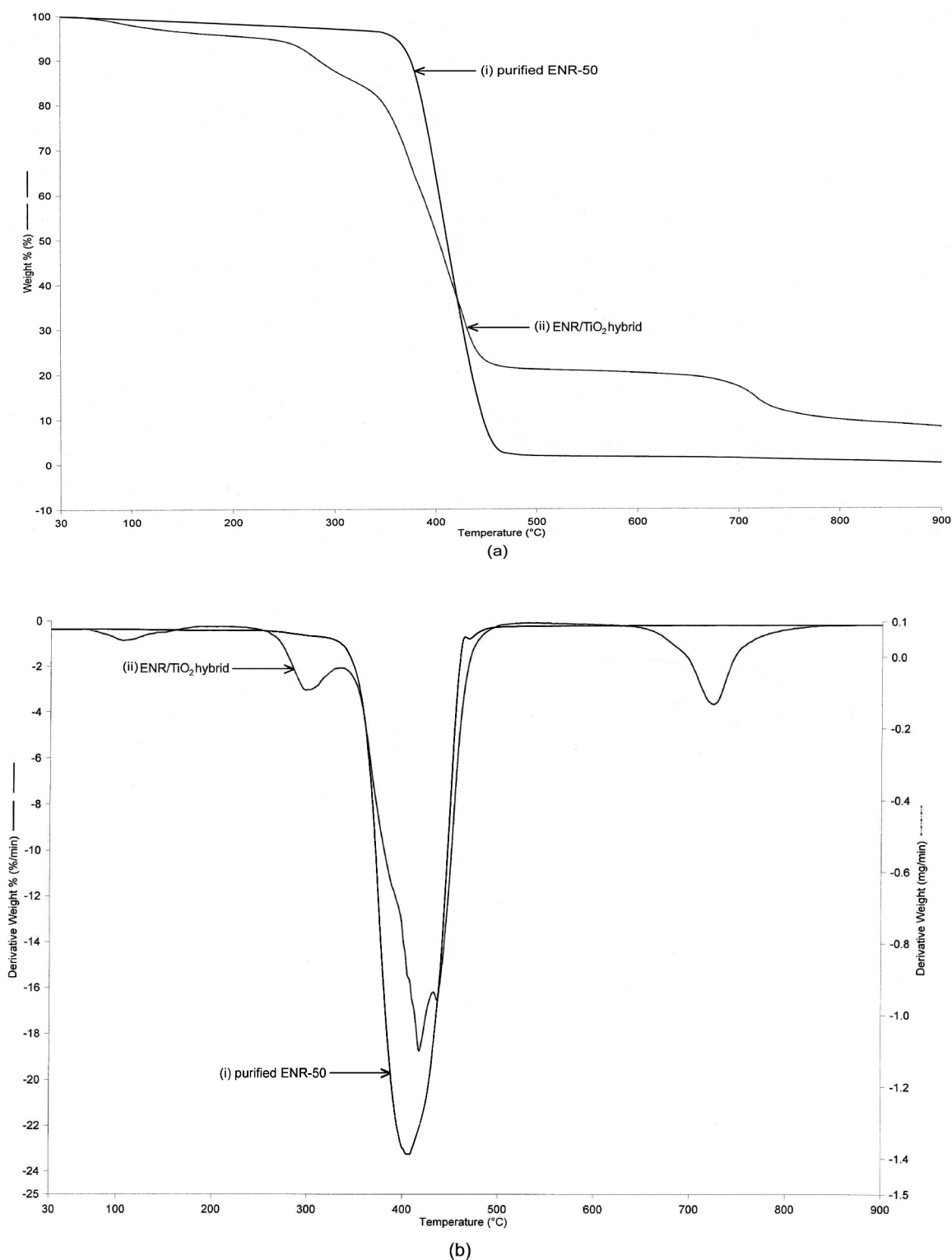
Fig. 7 (a) TG and (b) DTG thermograms of (i) purified ENR and (ii) ENR/TiO$_2$ hybrid.

the thermal degradation of the hybrid shifted to a lower temperature than purified ENR-50; there are a few possibilities occurring, such as the breakdown of the main chains of ENR-50, elimination reaction of certain organic groups and de-polymerization (Li et al., 1998). Typically, a relatively low

molecular mass organic molecule is stable at the temperature range of 100–200 °C (Brown, 2001) and requires low heat energy to break up its bond. However, the ENR chain distributes its energy along the polymer chains and thus can stabilize its chains to a higher temperature compared to simple
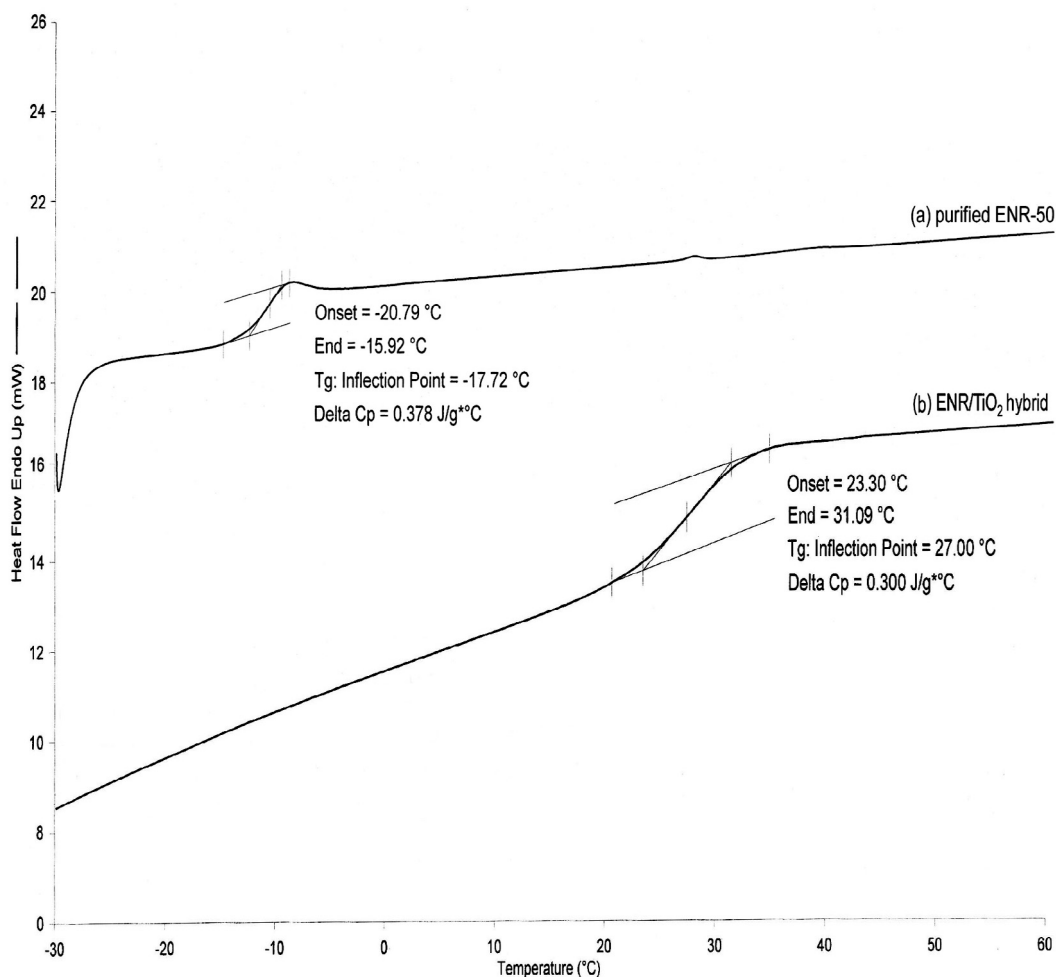
Fig. 8 DSC thermograms of (a) purified ENR and (b) ENR/TiO₂ hybrid.

organic molecules (Li et al., 1998). The fourth degradation is due to the rearrangement of the Ti—O—Ti skeleton to a discrete TiO₂ perovskite structure.

3.4. DSC

The differential scanning calorimetry (DSC) thermograms of purified ENR-50 and ENR/TiO₂ hybrid are depicted in Fig. 8. The result shows that both samples of rubber and hybrid have a single glass transition (T_g) during the test. However, the hybrid T_g at 27 °C was above the purified ENR-50 T_g at −17.72 °C (Çopuroğlu et al., 2006; Morselli et al., 2012). Generally, a single T_g indicates good miscibility and strong adhesion between both the polymer matrix and inorganic moieties (Morselli et al., 2012). A single T_g could also indicate that the hybrid behaves as a new polymer (Mas Haris and Raju, 2014). As mentioned earlier, the ring opening reaction percentage of epoxide groups in the hybrid is higher than that of purified ENR-50. This indicates that the Ti moieties influence the T_g value of the hybrid. The Ti moieties are able to limit and restrict the motion of polymer chains mobility via the formed crosslinking in the hybrid. Therefore, the hybrid remains in the rigid state at higher temperature compared with purified ENR-

50. However, the hybrid remains in the glassy state below the T_g value and in the rubbery state above T_g. The Ti content contributes to the free volume of the ENR-50. A high Ti content will reduce the free volume and limit the motion of polymer chains. By contrast, the polymer chains have relatively high free volume and are able to move easily at low Ti content. This can offer a strong interaction between the epoxide ring of ENR-50 and Ti moieties via the formed hybrid. A proper distance between Ti moieties and polymer chains helps in the hybrid formation (Rubab et al., 2014).

4. Conclusion

An ENR-50/TiO₂ hybrid in potassium hydroxide/isopropanol medium was produced via covalent bonds between the carbons of ring opened epoxide groups in ENR-50 and Ti precursors (C—O—Ti). The hybrid formation occurred at both the most and least hindered carbons of the ring-opened epoxide groups. Moreover, the presence of Ti moieties improved the thermal stability of the hybrid. This was in agreement with the finding of the DSC analysis, where Ti moieties restricted the mobility of polymer chains via the formed crosslinking in the hybrid.

Acknowledgement

References

Babazadeh, M., Rezazad Gohari, F., Olad, A., 2012. Characterization and physical properties investigation of conducting polypyrrole/TiO$_2$ nanocomposites prepared through a one-step "in situ" polymerization method. J. Appl. Polym. Sci. 123, 1922–1927.

Bakar, M.A., Ismail, J., Teoh, C.H., Tan, W.L., Bakar, N.H.H.A., 2008. Modified natural rubber induced aqueous to toluene phase transfer of gold and platinum colloids. J. Nanomater. 2008, 33.

Barlier, V., Bounor-Legaré, V., Alcouffe, P., Boiteux, G., Davenas, J., 2007. Formation of TiO$_2$ domains in Poly (9-vinylcarbazole) thin film by hydrolysis–condensation of a metal alkoxide. Thin Solid Films 515, 6328–6331.

Brown, M.E., 2001. Introduction to Thermal Analysis. Kluwer Academic Press, The Netherland, Techniques and Application.

Buzarovska, A., Grozdanov, A., 2012. Biodegradable poly (L-lactic acid)/TiO$_2$ nanocomposites: thermal properties and degradation. J. Appl. Polym. Sci. 123, 2187–2193.

Caldeira, L., Vasconcelos, D.C., Nunes, E.H., Costa, V.C., Musse, A.P., Hatimondi, S.A., Nascimento, J.F., Grava, W., Vasconcelos, W.L., 2012. Processing and characterization of sol–gel titania membranes. Ceram. Int. 38, 3251–3260.

Cao, J., Wang, L., He, X., Fang, M., Gao, J., Li, J., Deng, L., Chen, H., Tian, G., Wang, J., Fan, S., 2013. In situ prepared nano-crystalline TiO$_2$–poly (methyl methacrylate) hybrid enhanced composite polymer electrolyte for Li-ion batteries. J. Mater. Chem. A 1, 5955–5961.

Charpentier, P.A., Burgess, K., Wang, L., Chowdhury, R.R., Lotus, A.F., Moula, G., 2012. Nano-TiO$_2$/polyurethane composites for antibacterial and self-cleaning coatings. Nanotechnology 23, 425606.

Chen, H.J., Jian, P.C., Chen, J.H., Wang, L., Chiu, W.Y., 2007. Nanosized-hybrid colloids of poly (acrylic acid)/titania prepared via in situ sol–gel reaction. Ceram. Int. 33, 643–653.

Chiang, P.C., Whang, W.T., Tsai, M.H., Wu, S.C., 2004. Physical and mechanical properties of polyimide/titania hybrid films. Thin Solid Films 447, 359–364.

Conley, R.T., 1972. Infrared Spectroscopy. In: Qualitative Analysis. Allyn and Bacon Inc., Boston, pp. 92–200.

Çopuroğlu, M., O'Brien, S., Crean, G.M., 2006. Effect of preparation conditions on the thermal stability of an epoxy-functional inorganic–organic hybrid material system with phenyl side group. Polym. Degrad. Stab. 91, 3185–3190.

da Silva, A.F., Pepe, I., Gole, J.L., Tomás, S.A., Palomino, R., De Azevedo, W.M., da Silva Jr, E.F., Ahuja, R., Persson, C., 2006. Optical properties of in situ doped and undoped titania nanocatalysts and doped titania sol–gel nanofilms. Appl. Surf. Sci. 252, 5365–5367.

Dahham, O.S., Hamzah, R., Bakar, M.A., Zulkepli, N.N., Dahham, S.S., Ting, S.S., 2017. NMR study of ring opening reaction of epoxidized natural rubber in presence of potassium hydroxide/isopropanol solution. Polym. Test. 59, 55–66.

Dahham, O.S., Hamzah, R., Bakar, M.A., Zulkepli, N.N., Ting, S.S., Omar, M.F., Adam, T., Muhamad, K., Dahham, S.S., 2018. Synthesis and structural studies of an epoxidized natural rubber/titania (ENR-50/TiO$_2$) hybrid under mild acid conditions. Polym. Test. 65, 10–20.

Hamzah, R., Bakar, M.A., Dahham, O.S., Zulkepli, N.N., Dahham, S.S., 2016. A structural study of epoxidized natural rubber (ENR-50) ring opening under mild acidic condition. J. Appl. Polym. Sci. 133.

Han, C.C., Ismail, J., Kammer, H.W., 2004. Melt reaction in blends of poly (3-hydroxybutyrate-co-3-hydroxyvalerate) and epoxidized natural rubber. Polym. Degrad. Stab. 85, 947–955.

He, T., Zhou, Z., Xu, W., 2010. Thermal property of TiO$_2$–fluoropolymer fiber nanocomposites. J. Mater. Sci. 45, 2534–2537.

Judeinstein, P., Sanchez, C., 1996. Hybrid organic–inorganic materials: a land of multidisciplinarity. J. Mater. Chem. 6, 511–525.

Kango, S., Kalia, S., Celli, A., Njuguna, J., Habibi, Y., Kumar, R., 2013. Surface modification of inorganic nanoparticles for development of organic–inorganic nanocomposites – a review. Prog. Polym. Sci. 38, 1232–1261.

Lee, H.K., Ismail, J., Kammer, H.W., Bakar, M.A., 2005. Melt reaction in blends of poly (3-hydroxybutyrate)(PHB) and epoxidized natural rubber (ENR-50). J. Appl. Polym. Sci. 95, 113–129.

Li, S.D., Chen, Y., Zhou, J., Li, P.S., Zhu, C.S., Lin, M.L., 1998. Study on the thermal degradation of epoxidized natural rubber. J. Appl. Polym. Sci. 67, 2207–2211.

Lou, Y., Liu, M., Miao, X., Zhang, L., Wang, X., 2010. Improvement of the mechanical properties of nano-TiO$_2$/poly (vinyl alcohol) composites by enhanced interaction between nanofiller and matrix. Polym. Compos. 31, 1184–1193.

Lü, C., Yang, B., 2009. High refractive index organic–inorganic nanocomposites: design, synthesis and application. J. Mater. Chem. 19, 2884–2901.

Macwan, D.P., Dave, P.N., Chaturvedi, S., 2011. A review on nano-TiO$_2$ sol–gel type syntheses and its applications. J. Mater. Sci. 46, 3669–3686.

Mas Haris, M.R.H., Raju, G., 2014. Preparation and characterization of biopolymers comprising chitosan-grafted-ENR via acid-induced reaction of ENR50 with chitosan. eXPRESS Polym Lett. 8, 85–94.

Mishra, J.K., Chang, Y.W., Kim, D.K., 2007. Green thermoplastic elastomer based on polycaprolactone/epoxidized natural rubber blend as a heat shrinkable material. Mater. Lett. 61, 3551–3554.

Mohamad, Z., Ismail, H., Thevy, R.C., 2006. Characterization of epoxidized natural rubber/ethylene vinyl acetate (ENR-50/EVA) blend: effect of blend ratio. J. Appl. Polym. Sci. 99, 1504–1515.

Morselli, D., Bondioli, F., Sangermano, M., Messori, M., 2012. Photo-cured epoxy networks reinforced with TiO$_2$ in-situ generated by means of non-hydrolytic sol–gel process. Polymer 53, 283–290.

Nawi, M.A., Kean, L.C., Tanaka, K., Jab, M.S., 2003. Fabrication of photocatalytic TiO$_2$-epoxidized natural rubber on Al plate via electrophoretic deposition. App. Catal. B: Environ. 46, 165–174.

Noriman, N.Z., Ismail, H., Rashid, A.A., 2010. Characterization of styrene butadiene rubber/recycled acrylonitrile-butadiene rubber (SBR/NBRr) blends: the effects of epoxidized natural rubber (ENR-50) as a compatibilizer. Polym. Test. 29, 200–208.

Ochi, M., Nii, D., Suzuki, Y., Harada, M., 2010. Thermal and optical properties of epoxy/zirconia hybrid materials synthesized via in situ polymerization. J. Mater. Sci. 45, 2655–2661.

Ochi, M., Nii, D., Suzuki, Y., Harada, M., 2010. Thermal and optical properties of epoxy/zirconia hybrid materials synthesized via in situ polymerization. J. Mater. Sci. 45, 2655–2661.

Ouyang, G., Wang, K., Chen, X.Y., 2012. TiO$_2$ nanoparticles modified polydimethylsiloxane with fast response time and increased dielectric constant. J. Micromech. Microeng. 22, 074002.

Pandey, S., Mishra, S.B., 2011. Sol–gel derived organic–inorganic hybrid materials: synthesis, characterizations and applications. J. Sol-Gel Sci. Technol. 59, 73–94.

Rubab, Z., Afzal, A., Siddiqi, H.M., Saeed, S., 2014. Preparation, characterization, and enhanced thermal and mechanical properties of epoxy-titania composites. Scientific World J. 2014, 515739.

Sanchez, C., Julián, B., Belleville, P., Popall, M., 2005. Applications of hybrid organic–inorganic nanocomposites. J. Mater. Chem. 15, 3559–3592.

Sanchez, C., Shea, K.J., Kitagawa, S., 2011. Recent progress in hybrid materials science. Chem. Soc. Rev. 40, 471–472.

Tao, P., Li, Y., Rungta, A., Viswanath, A., Gao, J., Benicewicz, B.C., Siegel, R.W., Schadler, L.S., 2011. TiO$_2$ nanocomposites with high

refractive index and transparency. J. Mater. Chem. 21, 18623–18629.

Wen, J., Wilkes, G.L., 1996. Organic/inorganic hybrid network materials by the sol−gel approach. Chem. Mater. 8, 1667–1681.

Wetchakun, N., Phanichphant, S., 2008. Effect of temperature on the degree of anatase–rutile transformation in titanium dioxide nanoparticles synthesized by the modified sol–gel method. Curr. App. Phys. 8, 343–346.

Xiong, M., You, B., Zhou, S., Wu, L., 2004. Study on acrylic resin/titania organic–inorganic hybrid materials prepared by the sol–gel process. Polymer 45, 2967–2976.